

Effect of Aging Temperature on Plastic Flow Behaviour and Toughness of Nickel Free High Nitrogen Austenitic Stainless Steels

Krishna Kumar K^{a*} , Anburaj J^a, Subramanian R^a

^aPSG College of Technology, Department of Metallurgical Engineering, Coimbatore, 641 004, Tamilnadu, India.

Received: September 06, 2022; Revised: November 26, 2022; Accepted: January 9, 2023

In the present study, tensile properties, plastic flow behaviour and impact toughness of Nickel free High Nitrogen Austenitic Stainless Steels (NFHNSS) were evaluated under solution annealed and aged condition (at 700 °C, 800 °C and 900 °C for 14 hours). Plastic flow behaviour was analyzed using Holloman and Ludwigson flow equations. Samples in solution annealed and aged conditions exhibited a flow transition behaviour. Ludwigson flow equation produces best fit for flow transition behaviour. Transmission Electron Microscope (TEM) investigations of NFHNSS samples after tensile test revealed dislocation network and planar arrangement of dislocations adjacent to Grain Boundaries (GB) in the solution annealing and aged conditions respectively. Plastic deformation of NFHNSS occurs by a combination of planar glide and twinning. Impact energy was significantly higher in solution annealed condition than aged condition. Impact energy values decreased with increasing aging temperature. Precipitation and growth as well as morphology of Cr₂N at the GBs reduce the impact energy values significantly. Presence of larger precipitates readily pull out from GB easily than smaller precipitates at low temperatures. Large precipitate, at the GB's readily pull out at low temperature, compared to slower ones.

Keywords: High Nitrogen Austenitic Stainless Steels, plastic flow behaviour, dislocations, TEM, Ludwigson flow equation.

1. Introduction

In the recent years, NFHNSS are being extensively used in medical, offshore and oil field sectors, due to their outstanding metallurgical and mechanical properties. Mechanical and corrosion properties of austenitic stainless steels are markedly influenced by additions of Mn and N contents¹. Particularly at low temperatures, Mn substantially reduces the ductility and the impact toughness of austenitic stainless steels^{2,3}. Lee et al.⁴ reported the effect of Mn and N on deformation configuration and Stacking Fault Energy (SFE) of NFHNSS and hence the correlation between deformation microstructure and SFE in austenitic stainless steels. Lee and Choi⁵ showed that the Fe-12%Mn binary alloy has the minimum SFE and hence enhanced Transformation – Induced Plasticity (TRIP) effect. Alloy design for improvement of strength and impact energy of austenitic austenitic stainless steels with considerable amounts of Mn and N content was reported by Behjati et al.⁶. Nitrogen is a strong austenitic stabilizer and a potential element to increase the strength of austenitic stainless steels through solid solution strengthening without compromising its toughness and ductility^{2,6}.

A systematic analysis of the tensile and plastic flow behaviour of NFHNSS is necessary to optimize the microstructure and mechanical properties for critical engineering applications.

Several authors have proposed flow equations to establish the relationship between flow stress and true plastic strain⁷⁻¹⁰.

Plastic deformation region in flow curve of the metals can be expressed by the following power curve equation^{8,9}:

$$\sigma = K \varepsilon^n \quad (1)$$

Where, σ and ε are flow stress and true plastic strain respectively.

K and n are strength coefficient and strain hardening exponent respectively.

Ludwigson equation, a modified power curve equation, can be used to express the plastic deformation zone in the flow curve of austenitic stainless steels, other FCC alloys, and low stacking fault energy alloys¹⁰:

$$\sigma = K_1 \varepsilon^{n_1} + \exp(K_2 + \varepsilon n_2) \quad (2)$$

Where, K_1 and n_1 are constants calculated from power curve equation.

K_2 and n_2 are constants¹⁰.

It has been reported⁸⁻¹⁵ that the composition and the temperature of deformation of austenitic stainless steels influenced strain hardening behaviour and its relation to dislocations arrangement. Schröder et al.¹⁶ reported that Mn increase the ultimate tensile strength of metastable austenitic stainless steels. Quitzke et al.¹⁷ reported that influence of

*e-mail: kkk.metal@psgtech.ac.in

nitrogen on mechanical properties of high Mn austenitic stainless steel at -40°C . Mola et al.¹⁸ reported the dynamic strain aging mechanisms in a high Mn metastable austenitic stainless steel. Chen et al.¹⁹ reported the impact toughness and crack propagation behavior of in nickel free high Mn austenitic steel at -196°C .

This paper focuses on the effect of solution annealing and aging temperatures of on plastic flow behavior and impact properties Plastic flow behaviour of NFHNSS was determined from power curve Equation 1 and Ludwigson Equation 2 through linear and non-linear regression analysis using R-studio software. Factors like strength coefficient (K), strain hardening exponent (n) and strain hardening rate were determined to analyse the strain hardening behavior of NFHNSS samples in both solution annealed as well as aged conditions. Impact energy of NFHNSS samples was also measured under solution annealed as well as aged conditions. Fracture behaviour of impact tested samples (solution annealed as well as aged) were investigated using SEM.

2. Materials and Methods of Testing

Hot Rolled NFHNSS samples (composition as in Table 1) were solution annealed at 1100°C for 1 hour followed by water quenching to obtain a homogenous microstructure. Solution treated samples were further subjected to isothermal ageing at 700°C , 800°C and 900°C respectively for 14 hours. Tensile strength, yield strength and elongation of the solution annealed and aged NFHNSS were determined by a Instron Tensile machine of 100 kN capacity on specimens prepared as per ASTM E8 standard. An initial strain rate of $1 \times 10^{-4} \text{ s}^{-1}$ was used for all tensile tests. 15% deformed tensile specimens were used for studying the substructure analysis using TEM. The change in flow behaviour of NFHNSS was correlated with dislocation substructures observed in solution annealed and aged samples. Impact energy of the solution-annealed and aged samples was measured using a Charpy V-notched machine at room temperature and low temperature (-50°C) as per ASTM A370 standard.

3. Results and Discussion

3.1. Microstructural evaluation using TEM

Imaging and Selected Area Diffraction (SAD) modes were used to characterized the microstructure of NFHNSS in solution-annealed as well as specimen aged at 800°C for 14 hours. Bright Field TEM image showed the presence of austenite matrix in solution annealed sample while aged sample revealed a lamellar austenite structure (Figure 1a, 1c). Indexed SAD pattern (Figure 1b) of austenite matrix in solution annealed confirmed the zone axis close to $\langle 011 \bar{1} \rangle$. Similarly, indexed SAD pattern (Figure 1d) of the lamellar austenite in the aged sample at 800°C for 14 hours showed

zone axis close to $\langle 1\bar{1}0 \rangle$. The results of SAD patterns confirm that these two phases have FCC crystal structure with different crystal orientation.

As discussed in an earlier research work¹¹, microstructure of NFHNSS samples showed a fully austenitic structure with twins in the annealed condition while the coarse lammellar austenite was observed for all the aged specimens. Coarsening of lamellar austenite was relatively higher at 700°C aging temperature than that of 800°C and 900°C aging temperatures for aging time of 14 hours. In addition, the presence of chromium nitride precipitates (Cr_2N) was observed at the austenite grain boundaries of NFHNSS samples aged at 700°C , 800°C and 900°C . Morphology of these Cr_2N precipitates varied with aging temperature : discrete needle-like, lenticular and discrete disk of Cr_2N precipitates for specimens aged at 700°C , 800°C and 900°C respectively. It was also observed that the volume of precipitated increases with increasing aging temperature.

3.2. Plastic flow behaviour of NFHNSS in the heat treated conditions

Plastic flow behaviour of the NFHNSS under different heat treated conditions was evaluated using tensile tests. Stress – strain curves for the sample solution-annealed at 1100°C for 1 hour as well as aged at 700°C , 800°C and 900°C for 14 hours are shown in Figure 2.

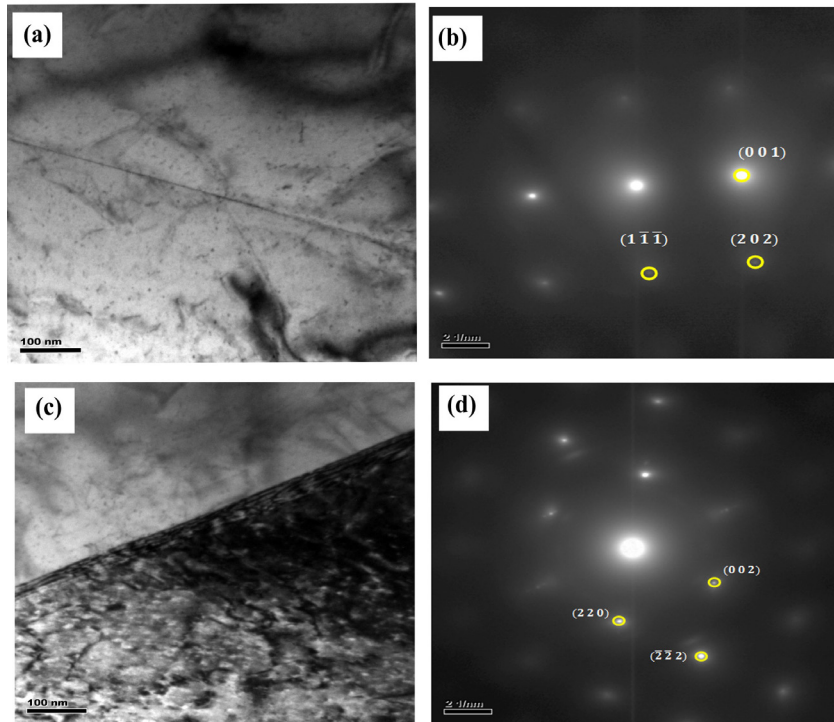
Ultimate Tensile Strength (UTS), Young's Modulus (YS), 0.2% offset Yield Stress (YS) and corresponding yield strain values of solution annealed and aged samples are given in Table 2. From the results, it can be observed that the solution annealed sample has the highest UTS of 905 MPa compared to other isothermally aged samples. This is due to the presence of homogenous microstructure containing fully austenitic matrix. In contrast to UTS, the YS and the Young's modulus of solution annealed sample and sample aged at 700°C are showed no such major variation. However, YS and Young's modulus of the samples aged at 800°C and 900°C were relatively lower compared to those aged at 700°C . At higher aging temperatures, precipitation of Cr_2N in the austenitic matrix results in a decrease in the UTS and YS of the NFHNSS due to the depletion of Cr and N solute atoms in austenite matrix. For samples aged 900°C for 14 hours, the stress-strain shifted downward indicating a reduction in tensile properties. It showed a decrease of nearly 14% UTS value for samples aged at 900°C compared to the annealed NFHNSS sample (Table 2). This could be due to the morphological change in Cr_2N precipitates at different aging temperatures. Size, shape and distribution of brittle Cr_2N phase has notable effect of hardness and tensile properties of the NFHNSS. On the other hand, presence of Cr and N, as solid solution strengthener in austenite led to an increase in the tensile strength for solution annealed samples. However, the depletion of Cr and N concentration

Table 1. Chemical composition of NFHNSS.

Composition (wt %)									
C	Si	Mn	S	P	Cr	Ni	Mo	N	Fe
0.03	0.33	21.54	0.005	0.018	17.81	0.08	0.14	0.56	Bal.

Table 2. Tensile properties of NFHNSS samples.

Sample ID	UTS (MPa)	Maximum Force [kN]	Modulus (Automatic Young's) [MPa]	Yield Strength (0.2% offset) [MPa]	Tensile strain (Displacement) at Yield (Offset 0.2%) [%]
Solution Annealing	905	27	81.60	576.38	0.90
700 °C	888	26	81.60	578.97	0.90
800 °C	875	30	74.80	499.89	0.86
900 °C	778	26	71.90	477.65	0.78

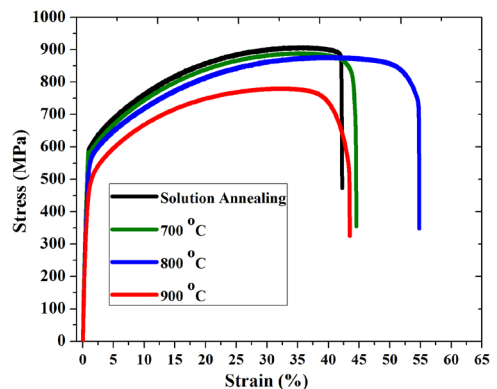

Figure 1. TEM Bright-Field images and SAD patterns for the austenitic matrix of sample solution annealed at 1100 °C for 1 hour (a and b) and lamellar austenite structure of the sample aged at 800 °C for 14 hours (c and d).

due to formation of Cr_2N precipitates in the matrix resulted in a decrease in the tensile strength.

True stress – true strain curves calculated for the samples solution-annealed at 1100 °C for 1 hour and aged at 700 °C, 800 °C and 900 °C for 14 hours (Figure 3) showed that sample aged at 900 °C showed a very limited plastic flow compared to the other ageing temperatures. Based on the Equation 1, log- log plots for flow stress and true plastic strain were constructed. Linear Regression analysis for the log-log plots were performed using R-studio software. From the y – intercept and slope of the log-log plots, K and n values of solution annealed and aged samples were obtained. Strain hardening rate of the samples were calculated using the following Equation 3⁷:

$$\text{Strain hardening rate} = n \frac{\sigma}{\varepsilon} \quad (3)$$

Linear regression fit results by power curve Equation 2 for samples at solution annealed and aged conditions are shown in Figure 4. R-square values for the linear fit are given in Table 3. R-square value above 0.9 indicates high


Figure 2. Stress – strain curves of the NFHNSS samples in solution annealed and aged condition.

level of correlation between predicted and measured values. Figure 4 shows the correlation between experimental and linear fit values. Values of K and n were calculated from

the slope and intercept values of linear regression fit lines respectively. K and n values of solution annealed as well as aged samples are given in Figure 5. From Figure 4, correlation between experimental and linear fit is high in high strain region (above 0.4) than low strain region (below 0.4). A large deviation from the linear fit to experimental values was observed in low strain regions. Hence, power curve equation cannot be used to find true stress values in low strain region. From Figure 4, it can be seen that a small positive deviation was observed in the intermediate strain region,

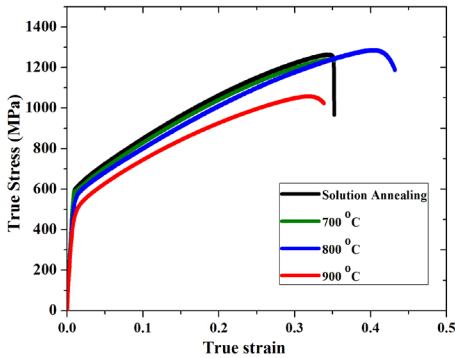


Figure 3. True stress – True strain curves of the NFHNSS samples in solution annealed and aged condition.

while a negative deviation was observed in the high strain regions. This variation in linear fit indicates the inability of the power curve equation to predict plastic flow behaviour for the entire range of stress- strain data. $\log(\text{true strain})$ increases slowly in a non-linear way during the initial stage and above a certain strain $\log(\text{true strain})$ increased linearly with strain. Average slope of high strain region is significantly higher than average slope of low strain region. This kind of two stage flow behavior is analyzed by Ludwigs Equation 2.

Non-linear regression analysis was performed by R studio software (using Ludwigs Equation 2) in order to obtain the best fit for experimental true stress – strain values. Constants K_2 and n_2 in the Ludwigs equation for the solution annealed and aged samples were determined from the $\ln(\Delta)$ Vs true plastic strain curve^{8,9}, where Δ is the determined from the following equation:

Table 3. Values of R^2 obtained from linear regression fit (power curve) and non-linear regression fit (Ludwigs curve).

Sample ID	Linear regression fit	Non-linear regression fit
Solution Annealing	0.9630	0.9995
700 °C	0.9627	0.9996
800 °C	0.9618	0.9993
900 °C	0.9810	0.9993

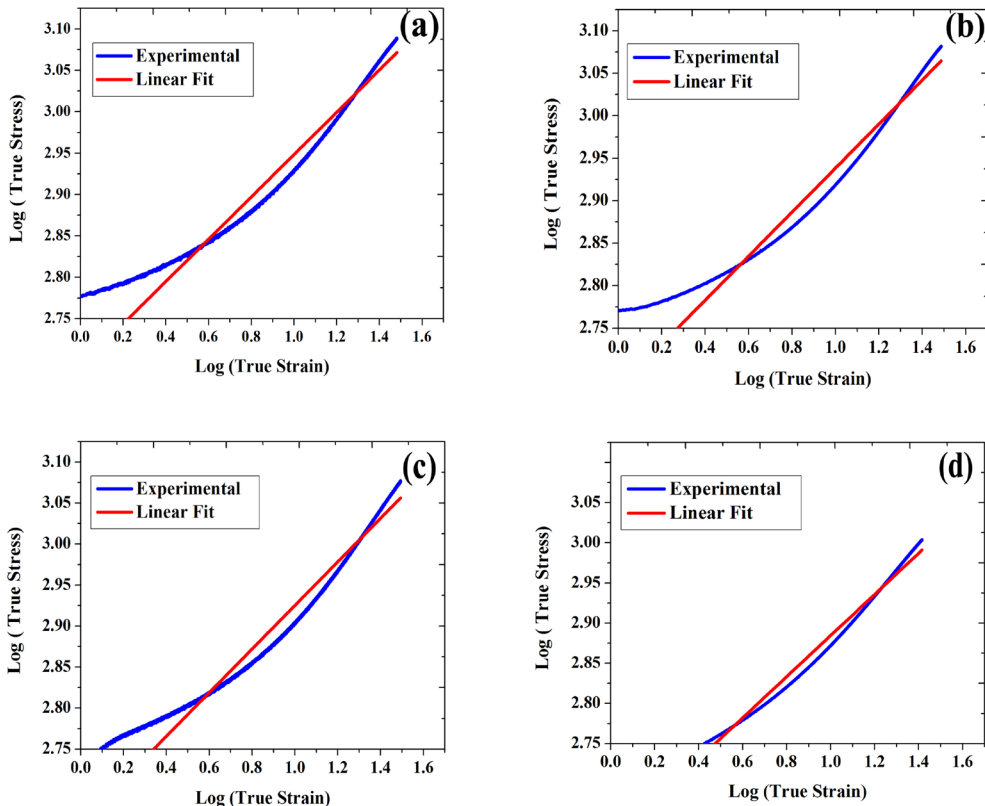


Figure 4. $\log(\text{True stress}) - \log(\text{True strain})$ plots of NFHNSS samples fitted in linear regression method (a) Solution annealed 1100 °C for 1 hour (b) aged 700 °C for 14 hours (c) aged 800 °C for 14 hours (D) aged 900 °C for 14 hours.

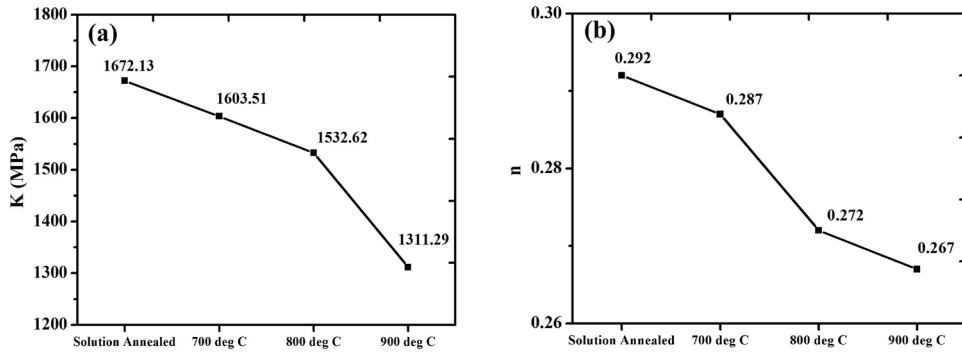


Figure 5. (a) Strength coefficient (K) values (b) Strain hardening (n) exponent values of the NFHNSS samples in solution annealed and aged condition.

$$\Delta = \left\{ \begin{array}{l} \text{Experimental True stress at low strain region} \\ \text{True stress determined from the extended} \\ \text{linear regression curve at low strain regions} \end{array} \right\} \quad (4)$$

Ludwigson constants K_2 and n_2 for all samples are calculated from the $\ln(\Delta)$ Vs true plastic strain curve (Figure 6) for low strain regions. Figure 7 illustrates the effect of solution annealing and aging temperature on flow parameters (K_2 and n_2) in the Ludwigson equation. Figure 8 shows the correlation between experimental and non-linear Ludwigson fit values. It can be observed that there is very little variation of Ludwigson fit to experimental values for all strain regions as indicated by a high R-square values of Ludwigson fits (Table 3).

Strain hardening rate of (solution annealed and aged NFHNSS) samples were plotted with respect to true stress and true strain (Figure 9). Strain hardening rate decreased rapidly during initial stage at a low stress and low strain for all the samples. However, strain hardening rates were almost constant later during high stress and high strain deformation stages. Both strain hardening rate Vs True stress and strain hardening rate Vs True strain curves were found to be similar. Strain hardening Vs true stress plots for solution annealed and aged samples were well separated while strain hardening Vs true stress plots were close to overlapping.

Strain rate of solution annealed sample was found to be higher than that of aged samples. Increasing aging temperature markedly decreased the strain hardening rate. High strain rate observed in solution annealed condition can be attributed to the fully homogenous austenite structure. However, the aged samples showed lower strain hardening rate since samples were subjected to isothermal ageing treatment. Concentration of Cr and N contents decreased in the austenite matrix with ageing treatment as a result of Cr_2N precipitates that develop in NFHNSS. Aging at 700 °C, 800 °C and 900 °C for 14 hours caused, the Cr and N elements to diffuse out of austenite matrix and to form Cr_2N precipitates. Increasing aging temperature led to an decrease in the solubility of Cr and N in the austenite and combining to form Cr_2N consequently reducing the flow parameter values. Thus it can be concluded that an increase in aging temperature reduces the strain hardening rate of NFHNSS alloy.

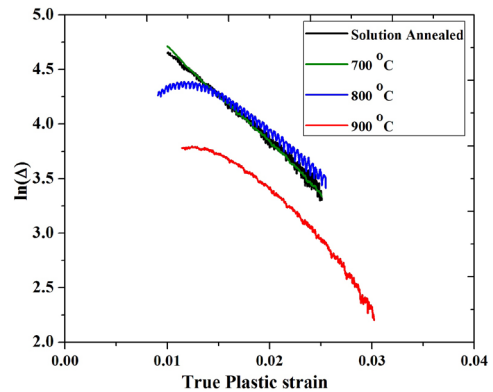


Figure 6. Determination of parameters in Ludwigson equation for solution annealed and aged NFHNSS samples.

The change in flow behaviour of NFHNSS can be related to the dislocation substructures observed in both solution annealed as well as aged sample. Bright Field TEM micrographs (Figure 10) show the variation in dislocation arrangements as a function of aging temperature. Samples solution annealed at 1100 °C, clearly revealed dislocation network (Figure 10a). Samples aged at 700 °C, 800 °C and 900 °C showed gradually increasing planar arrangement of dislocations, both close to GBs as well as within the austenite matrix. It has been reported that planar arrangement of dislocation occurs by a combination of planar glide and twinning⁷⁻⁹. In NFHNSS sample aged at 700 °C, a reduction in Cr and N content increase the stacking fault energy of austenite matrix compared to solution annealed sample. However, the dissolution of Cr and N was low compared to samples aged at 800 °C and 900 °C. Hence, a planar arrangement of dislocations are not proper but significant dislocation pile up at GBs were observed at samples aged at 700 °C (Figure 10b). In samples aged at 800 °C and 900 °C, high volume fraction of Cr_2N precipitates tends to decrease the Cr and N concentration in austenite matrix, which in turn significantly increases the stacking fault energy of the austenite matrix¹²⁻¹⁴. This leads to a planar arrangement of dislocation. It has been reported increasing aging times lead to formation of finer dislocation cell structure^{8,9}. These

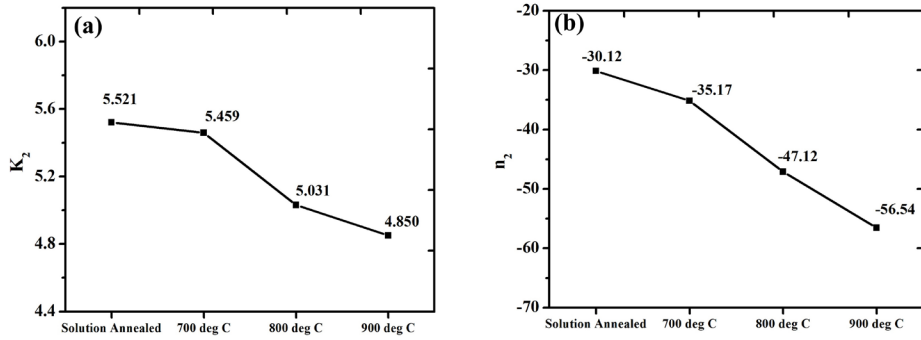


Figure 7. Ludwison parameters (a) K_2 and (b) n_2 values for solution annealed and aged NFHNS samples.

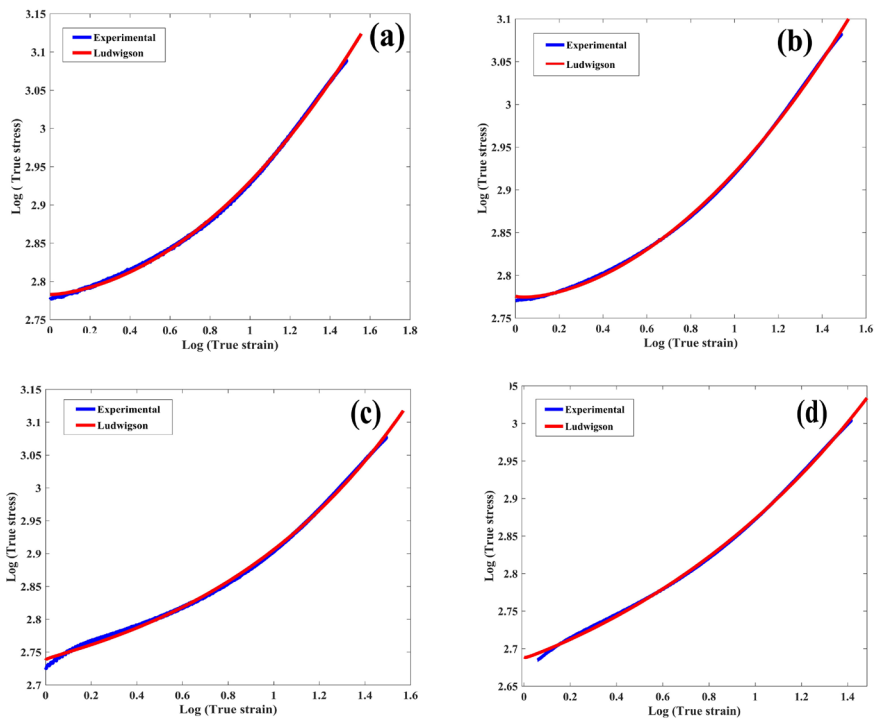


Figure 8. Log (True stress) – log (True strain) plots of NFHNS samples fitted using Ludwison equation (a) Solution annealed 1100 °C for 1 hour (b) aged 700 °C for 14 hours (c) aged 800 °C for 14 hours (D) aged 900 °C for 14 hours.

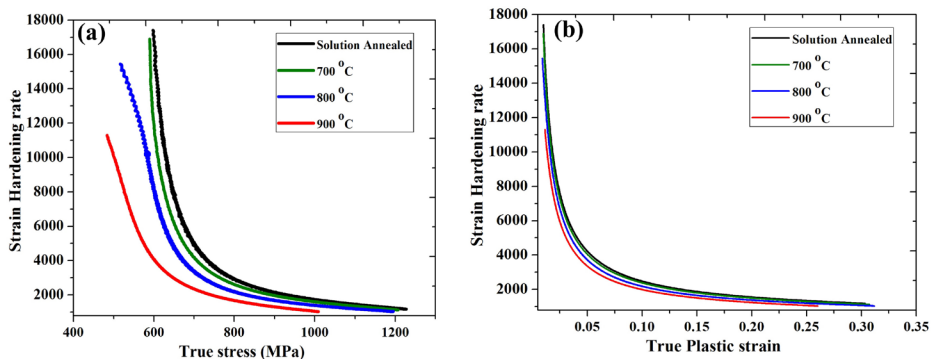


Figure 9. (a) Strain hardening rate Vs true stress (b) Strain hardening rate Vs true plastic strain plots for NFHNS samples at solution annealed and aged conditions.

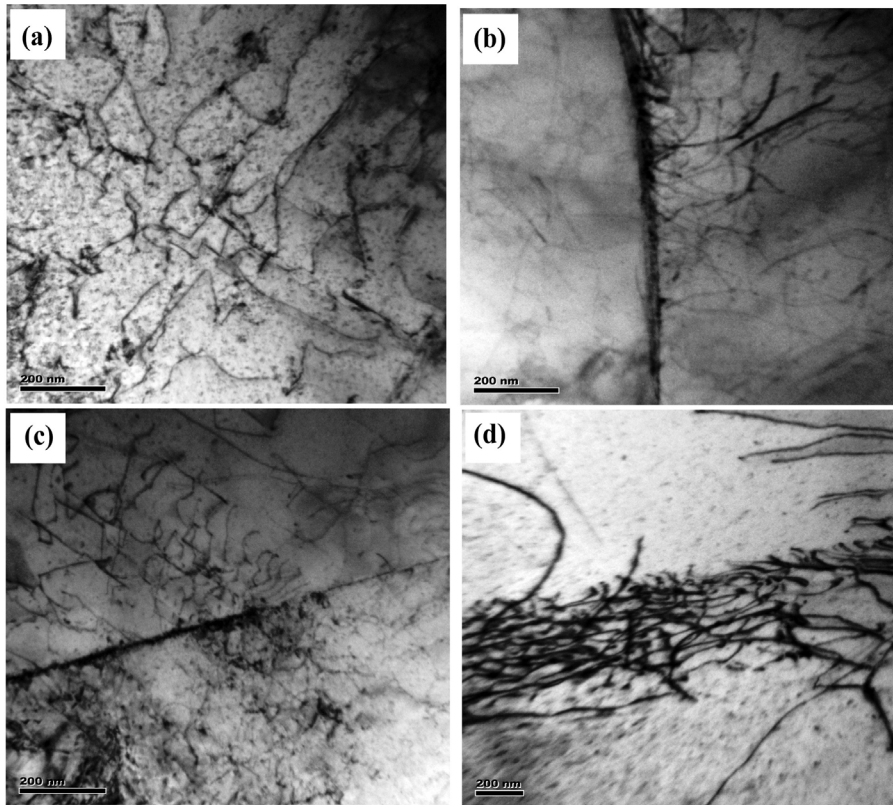


Figure 10. Bright field TEM micrographs of dislocations morphologies of NFHNSS samples (a) Solution annealed 1100 °C for 1 hour (b) aged 700 °C for 14 hours (c) aged 800 °C for 14 hours (D) aged 900 °C for 14 hours.

dislocation structures affect the strain hardening behavior of NFHNSS samples aged at higher aging temperatures.

3.3. Impact toughness of NFHNSS

V-notch Charpy impact tests were performed for solution annealed and 700 °C, 800 °C and 900 °C aged NFHNSS samples at room temperature and sub-zero temperature (-50 °C). The room temperature impact test result is shown in Figure 11a. Average impact energy obtained for samples in solution annealed as well as 700, 800 and 900 °C at room temperature were as 210 J, 178 J, 151 J and 139 J respectively. From these results, it can be concluded that the impact energy of solution annealed condition was significantly higher compared to the aged samples. Impact energy of the NFHNSS decreased with increasing aging temperature and lowest impact energy was observed in the samples aged at 900 °C which could be attributed to the presence of Cr₂N precipitates.

Fracture surfaces of the impact samples of NFHNSS at higher aging temperatures were subjected to SEM investigations to understand the fracture behavior with reference microstructure of the aged samples. SEM micrographs of the fractured surfaces of solution annealed and aged impact samples is shown in Figure 12. The fractured surface of solution annealed impact tested sample showed a mixed mode (ductile and brittle) with inter crystalline fracture, as seen from in Figure 12a. It can also be observed that the solution-

annealed sample showed the presence of some micro voids at dimples. These micro voids subsequently coalesced to form a crack. Further propagation of these cracks perpendicular to the direction of the loading resulted in the final failure.

Impact fracture surface of sample aged at 700 °C also showed a mixed ductile and brittle mode inter crystalline fracture (Figure 12b). However, the ductile fracture mode was more predominant in the solution annealed condition. On other hand, the brittle fracture mode was predominant in the sample aged at 700 °C. Fracture surface of samples aged at 800 °C and 900 °C showed a fully cleavage mode fracture confirming brittle failure. The cleavage facets is found to be significantly larger in the brittle fracture regions. Formation of large Cr₂N precipitates and its decohesion from the matrix during impact loading, pile-up of dislocations at GBs and formation high local stresses causes the active deformation planes leading to brittle failure [2,3,8 & 9].

Figure 11b shows the the impact energy of samples at -50 °C. The average impact energy values of 152 J, 121 J, 105 J and 93J were obtained for the samples at solution annealed, 700 °C, 800 °C and 900 °C aging temperatures respectively. The impact energy value of solution annealed sample was significantly higher in comparison to the aged samples. As aging temperature increased, from 700 °C to 900 °C, the impact energy of the samples decreased significantly. The lowest impact energy value was observed 900 °C aged samples. Impact energy values at -50 °C were

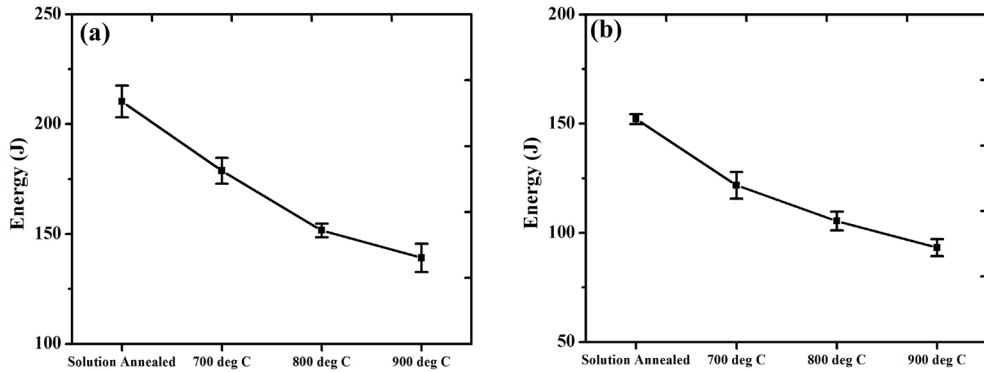


Figure 11. Charpy impact energy values of NFHNSS samples at (a) room temperature (b) -50 °C for solution annealed and aged conditions.

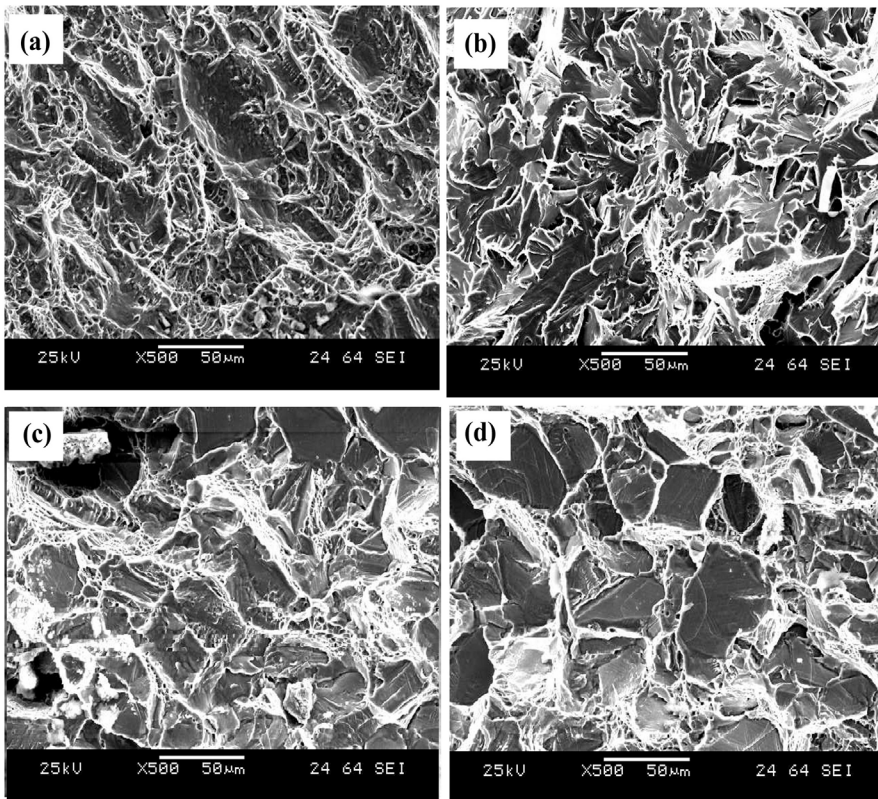


Figure 12. Fracture surfaces of NFHNSS Charpy V notch samples at room temperature (a) Solution annealed 1100 °C for 1 hour (b) aged 700 °C for 14 hours (c) aged 800 °C for 14 hours (D) aged 900 °C for 14 hours.

significantly lower (25–30%) compared to room temperature values. SEM micrographs of the fracture surfaces of the impact samples tested at -50 °C (Figure 13) showed that the fracture surface of solution annealed sample exhibited a mixed (ductile and brittle) mode inter crystalline fracture (Figure 13a). The fracture surface of sample aged at 700 °C for 14 hours also showed the ductile and brittle mixed mode inter crystalline fracture shown in Figure 13b. However brittle fracture was predominant in 700 °C aged sample. Fracture surface of samples aged at 800 °C and 900 °C showed almost

cleavage fracture indicating brittle mode of failure. Cracks were observed along the grain boundaries.

Precipitation, growth and morphology of Cr_2N at the GBs can predominantly reduce the impact energy values of NFHNSS. Presence of larger precipitates facilitated easy pull out from GB than smaller precipitates at low temperatures. This reduction in cohesive strength leads to reduction of bond strength¹⁵. Cracks may initiate due to pull out of precipitates from GBs^{3,15} and propagate along GBs. These intergranular cracks confirm the brittle mode of failure at low temperatures.

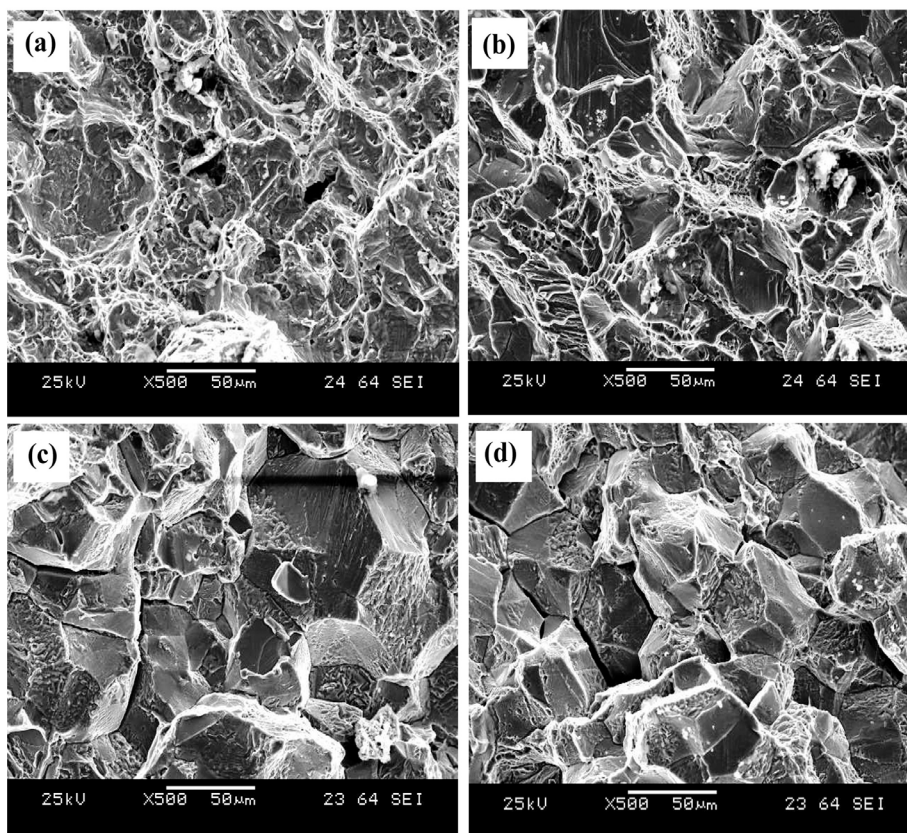


Figure 13. Fracture surfaces of NFHNSS Charpy V samples at $-50\text{ }^{\circ}\text{C}$ (a) Solution annealed $1100\text{ }^{\circ}\text{C}$ for 1 hour (b) aged $700\text{ }^{\circ}\text{C}$ for 14 hours (c) aged $800\text{ }^{\circ}\text{C}$ for 14 hours (D) aged $900\text{ }^{\circ}\text{C}$ for 14 hours.

4. Conclusions

Major conclusions drawn from the present work are:

- (1) NFHNSS has good stability to retain mechanical properties upto $700\text{ }^{\circ}\text{C}$ aging temperature, as there were no major differences in mechanical properties of solution-annealed and $700\text{ }^{\circ}\text{C}$ aged samples. However, YS and Young's modulus found to decrease significantly for samples aged at $800\text{ }^{\circ}\text{C}$ and $900\text{ }^{\circ}\text{C}$ due to depletion of Cr and N solute atoms in austenite matrix due to formation of Cr_2N precipitates.
- (2) Strain hardening rate of NFHNSS alloy in solution annealed condition was found to be higher than that of aged samples. Increasing the aging temperature led to a relative decrease with strain hardening rate. This is due to entire Cr and N content presents as in solid solution in the austenite matrix. Increasing aging temperature increases the dissolution of Cr and N elements from the matrix leading to a reduction in flow parameters. Hence increasing aging temperature reduces the strain hardening behavior of NFHNSS alloy.
- (3) Change in the flow behaviour of NFHNSS can be interrelated with dislocation substructures observed in solution annealed and aged condition. Solution annealed sample has dislocation network while aged samples show planar arrangement of dislocations

neener to GBs and as well as in austenite matrix. Plastic deformation of NFHNSS occurred by a combination of planar glide and twinning. Reduction of Cr and N content significantly increased the Stacking Fault Energy of the austenite matrix. This led to the formation of planar arrangement of dislocation. Increasing aging time, led to formation of finer dislocation cell structure. These dislocation structures affect the strain hardening behavior of NFHNSS at higher aging temperatures.

- (4) The impact energy of solution annealed sample was significantly higher than aged samples. Impact energy of these samples decreased with increasing aging temperature. Impact energy values at $-50\text{ }^{\circ}\text{C}$ were significantly lower (25 – 30%) compared to room temperature values. The presence of precipitates as well as growth and morphology of Cr_2N at the GBs can significantly reduce the impact energy values of NFHNSS.

5. References

1. Talha M, Behera CK, Sinha OP. A review on nickel-free nitrogen containing austenitic stainless steels for biomedical applications. *Mater Sci Eng C*. 2013;33(7):3563-75.
2. Pettersson N, Frisk K, Fluch R. Experimental and computational study of nitride precipitation in a CrMnN austenitic stainless steel. *Mater Sci Eng A*. 2017;684:435-41.

3. Milititsky M, Matlock DK, Regully A, Dewispelaere N, Penning J, Hanninen H. Impact toughness properties of nickel-free austenitic stainless steels. *Mater Sci Eng A*. 2008;496(1-2):189-99.
4. Lee TH, Kim SJ, Takaki S. Time-temperature-precipitation characteristics of high-nitrogen austenitic Fe-18Cr-18Mn-2Mo-0.9N steel. *Metall Mater Trans, A Phys Metall Mater Sci*. 2006;37(12):3445-54.
5. Lee YK, Choi C. Driving force for $\gamma \rightarrow \epsilon$ martensitic transformation and stacking fault energy of γ in Fe-Mn binary system. *Metall Mater Trans, A Phys Metall Mater Sci*. 2000;31(2):355-60.
6. Behjati P, Kermanpur A, Najafizadeh A, Samaei Baghbadorani H, Karjalainen LP, Jung JC, et al. Design of a new Ni-free austenitic stainless steel with unique ultra high strength-high ductility synergy. *Mater Des*. 2014;63:500-7.
7. Shao CW, Shi F, Li XW. Cyclic deformation behavior of Fe-18Cr-18Mn-0.63N nickel-free high-nitrogen austenitic stainless steel. *Metall Mater Trans, A Phys Metall Mater Sci*. 2015;46A(4):1610-20.
8. Karthik B, Veerababu R, Satyanarayana DVV. Effect of aging and oxidation on strain hardening behaviour of a nickel-free high nitrogen austenitic stainless steel. *Met Mater Int*. 2016;22(3):413-23.
9. Sun G, Zhang Y, Sun S, Hu J, Jiang Z, Ji C, et al. Plastic flow behavior and its relationship to tensile mechanical properties of high nitrogen nickel-free austenitic stainless steel. *Mater Sci Eng A*. 2016;662:432-42.
10. Ludwigson DC. Modified stress-strain relation for FCC metals and alloys. *Metall Trans, A, Phys Metall Mater Sci*. 1975;2(10):2825-8.
11. Krishna Kumar K, Anburaj J, Dhanasekar R, Satishkumar T, Abuthakir J, Manikandan P, et al. Kinetics of Cr_2N precipitation and its effect on pitting corrosion of Nickel-Free High-Nitrogen Austenitic Stainless Steel. *J Mater Eng Perform*. 2020;29(9):6044-52.
12. Mosecker L, Saeed-Akbari A. Nitrogen in chromium-manganese stainless steels: a review on the evaluation of stacking fault energy by computational thermodynamics. *Sci Technol Adv Mater*. 2013;14(3):1-14.
13. Lee T-H, Shin E, Oh C-S, Ha H-Y, Kim S-J. Correlation between stacking fault energy and deformation microstructure in high-interstitial-alloyed austenitic steels. *Acta Mater*. 2010;58(8):3173-86.
14. Anburaj J, Nazirudeen SSM, Narayanan R, Anandavel B, Chandrasekar A. Ageing of forged super austenitic stainless steel: precipitate phases and mechanical properties. *Mater Sci Eng A*. 2012;535:99-107. <http://dx.doi.org/10.1016/j.msea.2011.12.048>.
15. Fang L, Zhao W, Wei Y, Zhang Q, Zhang L, Ali N, et al. Characterization of dislocation structure in a Nb-bearing austenitic stainless steel after low cycle fatigue via TEM and EBSD. *Mater Res*. 2022;25:e20210401.
16. Schröder C, Volkova O, Wendler M. Influence of strain rate on the tensile properties of metastable austenitic stainless CrNi and CrMnNi spring steels. *Mater Sci Eng A*. 2022;850:143507.
17. Quitzke C, Schroder C, Ullrich C, Mandel M, Krüger L, Volkova O, et al. Evaluation of strain-induced martensite formation and mechanical properties in N-alloyed austenitic stainless steels by in situ tensile tests. *Mater Sci Eng A*. 2021;808:140930.
18. Mola J, Luan G, Huang Q, Ullrich C, Volkova O, Estrin Y. Dynamic strain aging mechanisms in a metastable austenitic stainless steel. *Acta Mater*. 2021;212:116888.
19. Chen J, Li S, Ren J, Liu Z. Quasi-in-situ observations of crack propagation and microstructure evolution of high manganese austenitic steel at -196°C . *Eng Fract Mech*. 2022;268:108509.